

# Structure and polarization properties of water: Molecular dynamics with a nonadditive intermolecular potential

I. Shvab and Richard J. Sadus\*

*Centre for Molecular Simulation, Swinburne University of Technology, P.O. Box 218, Hawthorn, Victoria 3122, Australia*

(Received 18 February 2012; revised manuscript received 23 April 2012; published 30 May 2012)

The temperature and density dependence of the structure and polarization properties of bulk water were systematically investigated using the *ab initio* MCYna potential [Li *et al.*, *J. Chem. Phys.* **127**, 154509 (2007)], which includes nonadditive contributions to intermolecular interactions. Molecular dynamics simulations were conducted for isochores of 1, 0.8, and 0.6 g/cm<sup>3</sup> and temperatures from 278 to 750 K. Special attention was paid to the structural change of water in the range from the normal boiling point to supercritical temperatures. At temperatures below the normal boiling temperature, water exhibits a tetrahedral structure along the 0.8 and 0.6 g/cm<sup>3</sup> isochores. A significant collapse of the hydrogen bonding network was observed at temperatures of 450, 550, and 650 K. The MCYna potential was able to successfully reproduce the experimental dielectric constant. The dielectric constant and average dipole moments decrease with increasing temperature and decreasing density due to weakened polarization. A comparison is also made with SPC-based models.

DOI: [10.1103/PhysRevE.85.051509](https://doi.org/10.1103/PhysRevE.85.051509)

PACS number(s): 61.20.-p, 31.15.xv, 61.25.Em, 05.20.-y

## I. INTRODUCTION

It is well known [1–4] that water exhibits a number of unusual properties such as density maximum and isothermal compressibility minimum at normal conditions, volume contraction under melting conditions, at least 15 crystalline polymorphs, and a high dielectric constant. Water is the most abundant substance in nature and knowledge of its thermodynamic and electrostatic properties is very important to understanding phenomena in fields such as protein crystallization and folding, biological membranes, electrolyte solutions, detergency, and metal extraction. In some cases these properties must be known to the utmost precision, requiring robust experimental techniques, theoretical studies, and molecular simulations.

The purpose of this work is to examine the effects of temperature and density on the structure and dynamics of bulk water for a wide range of states using molecular dynamics (MD) calculations. Most of the peculiarities of water behavior are ascribed to the hydrogen bond (H-bond) and the ability of water molecules to form three-dimensional networks. The fluid structure of water has been characterized by atomic pair correlation functions: oxygen-oxygen, oxygen-hydrogen, and hydrogen-hydrogen pair correlation functions. At ambient conditions, the first peak of the oxygen-hydrogen radial distribution function (RDF) around 1.8 Å is a manifestation of hydrogen bonding between molecules. Despite some ambiguity in H-bond definition, computer calculations with common empirical intermolecular potentials have successfully reproduced this hydrogen-bonding peak for ambient water. [1,5–7]

To investigate the properties of the hydrogen bonds at extreme conditions, studies have been extended to the supercritical state [8–13]. The region of supercritical temperatures and pressures is where most of the discrepancy between MD data and experiments arises. The *ab initio* calculations of Kang

*et al.* [9] indicate a conservation of 50% of H-bonds above 800 K. Molecular dynamics calculation with the TIP4P [13] model indicated that 70% of the hydrogen bonds found at ambient conditions remain at temperatures up to 1130 K. However, neutron diffraction experiments using the isotopic substitution technique (NDIS) of Soper [14] show that the first peak of the oxygen-hydrogen RDF completely disappears in the supercritical state at 673 K and densities of 0.58 and 0.66 g/cm<sup>3</sup>. This suggests that the hydrogen bonding network does not exist at supercritical conditions despite the fact that the hydrogen-bonding energy is well above the thermal energy at 673 K. Tromp *et al.* [15] suggested that the reason for this discrepancy is due to the deficiency of pairwise additive potentials such as TIP4P. Alternatively, Loffler *et al.* [16] claimed that the discrepancy arises from the inelasticity correction to the neutron data, which is particularly large for the light water sample. Recent *in situ* x-ray diffraction (XRD) experiments of Ikeda *et al.* [12] and Weck *et al.* [17] are in better agreement with the calculated results. However, calculations and experiments still provide a different description of hydrogen bonding in water at elevated temperatures and pressures.

Arguably, electrostatic interactions are the most important contribution to intermolecular interactions in water. The properties of water are most commonly obtained using fixed-point charge models [6,13]. Typical examples are the SPC/E [6] and TIP4P [13] models. The parameters for such potentials are optimized to reproduce the properties of liquid water at ambient conditions, i.e., a temperature of 298 K and a density of 1 g/cm<sup>3</sup>. The dipole moment of an isolated water molecule is 1.85 D. However, in condensed phases, the electrostatic field from the other molecules reorganizes the charge distribution. The average total dipole moment of ice Ih from self-consistent induction calculations is 3.09 D [18]. In the fluid phase, the dipole moment must have intermediate values between those in the gas and the ice. Therefore, it is not sufficient to describe the properties of water over a wide range of physical states using this kind of fixed-charge potential model. Instead, a realistic model should include the

\*rsadus@swin.edu.au

polarization effect of the molecule to describe the intermolecular interaction in the sub- and supercritical states. Car-Parrinello *ab initio* MD [19] is one of the best methods to account for the state dependence of intermolecular interactions. Kang *et al.* [9] and Dyer *et al.* [10] reported a first principle study of sub- and supercritical water. These workers calculated the structure factors and polarization distribution in water. However, the method used is computationally expensive and involves a very small number of particles (32–64 molecules). We need simpler models to investigate the properties of water over a wide range of thermodynamic states. A natural improvement of the empirical potential models is to explicitly introduce nonadditive many-body interactions such as three-body and polarizable contributions.

In this work, we apply an *ab initio* MCYna potential model [1] for investigation of structural and polarization properties of bulk water and compare results with the previous *ab initio* and MD results as well as with available experimental data. This model was introduced by Li *et al.* [1] and contains an *ab initio* description of two-body additive interactions plus nonadditive contributions from both three-body interactions and polarization. The nonadditive multibody influence arises because the induced dipole of each molecule generates an electric field that affects all other molecules. The molecular induced dipole moments are determined self-consistently with the electrostatic field reflecting the configuration of the fluid that depends on the physical state. A comparison is also made with SPC-based potentials.

## II. THEORY

### A. Intermolecular potential

The structure of the MCYna water molecule is shown in Fig. 1. Following the rigid model concept, each atomic nucleus is also the mass center of the atom. Point charges are assigned to the defined charge sites H and M, which might be different from the nucleus position (site M). In the given model, a positive charge  $q$  is placed on both H sites, and negative charge of  $2q$  is assigned to the M site. All values are given in the Table I.

The intermolecular potential  $U(r)$  for the system of  $N$  molecules is the sum of two-body additive  $u_2$  and nonadditive three-body  $u_3$  and polarizable  $u^{\text{pol}}$  contributions:

$$U(r) = \sum_{i<j}^N u_2(r_i, r_j) + \sum_{i<j<k}^N u_3(r_i, r_j, r_k) + u^{\text{pol}}. \quad (1)$$

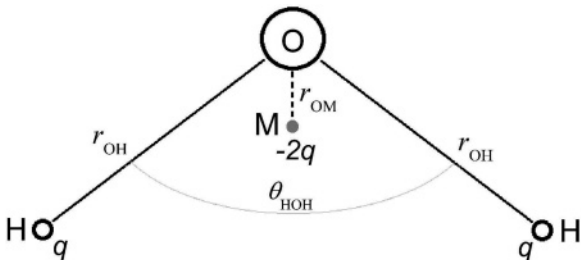


FIG. 1. Structure of the MCYna water molecule.

TABLE I. Intermolecular parameters used in the MCY and MCYna intermolecular potentials. Unless otherwise stated, all values are in atomic units.

Parameter value	
$a_1$	1734.1960
$a_2$	2.726696
$a_3$	1.061887
$a_4$	1.460975
$b_1$	2.319395
$b_2$	1.567367
$b_3$	0.436060
$b_4$	1.181792
$q^2$	0.514783
$r_{\text{OH}}$	0.957200
$r_{\text{OM}}$	0.505783
$\theta_{\text{HOH}}$ (deg)	104.52
$\alpha$ ( $\text{\AA}^3$ )	1.44
$\nu$	287.944

### 1. Additive two-body terms

The contribution of two-body interactions was obtained from the *ab initio* Matsuoka-Clementi-Yoshimine (MCY) potential [18]:

$$u_2 = q^2 \left( \frac{1}{r_{13}} + \frac{1}{r_{14}} + \frac{1}{r_{23}} + \frac{1}{r_{24}} \right) + \frac{4q^2}{r_{78}} - 2q^2 \left( \frac{1}{r_{18}} + \frac{1}{r_{28}} + \frac{1}{r_{37}} + \frac{1}{r_{47}} \right) + a_1 e^{(-b_1 r_{56})} + a_2 (e^{(-b_2 r_{13})} + e^{(-b_2 r_{14})} + e^{(-b_2 r_{23})} + e^{(-b_2 r_{24})}) + a_3 (e^{(-b_3 r_{16})} + e^{(-b_3 r_{26})} + e^{(-b_3 r_{35})} + e^{(-b_3 r_{45})}) - a_4 (e^{(-b_4 r_{16})} + e^{(-b_4 r_{26})} + e^{(-b_4 r_{35})} + e^{(-b_4 r_{45})}). \quad (2)$$

The meaning of the parameters is the same as given in the literature [1,20] and their values are given in Table I. The benefit of an *ab initio* potential is that it should avoid many of the theoretical uncertainties of empirical intermolecular potentials, such as the need to fit the parameters of the potential to experimental data for various properties.

### 2. Nonadditive terms

In general, nonadditive contributions to intermolecular interactions arise for induction interactions, resulting from molecular polarizability, short-range repulsion, and dispersion interactions. It is well documented [1,21] that multibody dispersion interactions can be adequately described using the Axilrod-Teller [22] triple dipole term,

$$u_3 = \frac{\nu(1 + 3 \cos \theta_i \cos \theta_j \cos \theta_k)}{(r_{ij} r_{ik} r_{jk})^3}, \quad (3)$$

where  $\theta_i$ ,  $\theta_j$ , and  $\theta_k$  are inside angles of the triangle formed by three atoms denoted by  $i$ ,  $j$ , and  $k$ , and  $r_{ij}$ ,  $r_{ik}$ , and  $r_{jk}$  are the three side lengths of the triangle. The parameter  $\nu$  is the nonadditive coefficient, which can be determined from experiment [23]. The theoretical background and rationale for this formula are given elsewhere [1]. The contribution of multibody nonadditive interactions from polarization was

obtained from [24]

$$u^{\text{pol}} = -\frac{1}{2} \sum_{i=1}^n \mu_i^{\text{int}} E_i^o, \quad (4)$$

where  $E_0$  is the electrostatic field of surrounding charges, and  $\mu_i^{\text{int}}$  is the induced dipole at site  $i$  given by

$$\mu_i^{\text{ind}} = \alpha\beta E_i = \alpha\beta \left[ E_i^o + \sum_{j=1, j \neq i}^N T_{ij} \mu_j^{\text{ind}} \right]. \quad (5)$$

In Eq. (5),  $\alpha\beta$  is the polarizability, and  $T_{ij}$  is the dipole tensor given by

$$T_{ij} = \frac{1}{4\pi\epsilon_0 r_{ij}^5} [3r_{ij}r'_{ij} - r_{ij}^2]. \quad (6)$$

To simplify the calculation, intramolecular interactions are not considered, which means that the induced dipole has no interaction with the partial charges on the same water molecule. Using a gas phase polarizability coefficient of  $1.44 \text{ \AA}^3$  from the literature [25], we obtained a dipole moment that significantly exceeded the 2.95–3 D range reported from *ab initio* MD and experiment [24]. To improve the calculation of the induced dipole, we scaled the polarizability coefficient by a factor of  $\beta = 0.557503$ . This means that the actual polarizability term is  $\alpha\beta = 0.802804 \text{ \AA}^3$ . This resulted in a dipole moment of 2.9 D, with 0.9 D attributed to induction interactions. To the best of our knowledge, there is no reliable experimental data of dipole moment for densities of 0.8 and  $0.6 \text{ g/cm}^3$ . Therefore, we have chosen values of the polarization constants  $\alpha\beta$  for  $\rho = 0.8$  and  $0.6 \text{ g/cm}^3$  to match with experimental values of dielectric constants. For these cases, the values of  $\beta$  are 0.348441 and 0.250878, respectively. The contribution of induction to the overall energy is 30%, which is consistent with estimates in the literature [26].

## B. Properties calculated

### 1. Structural properties

The structure of water was investigated by calculating the radial distribution function (RDF)  $g(r)$  from the following formula [25]:

$$g(r) = \frac{V}{4\pi\rho^2 N(N-1)} \left\langle \sum_i n_i(r) \Delta r \right\rangle, \quad (7)$$

where  $V$  is the system volume, and  $n(r)\Delta r$  is the number of particles that exist in the region between  $r$  and  $r+\Delta r$ . For polyatomic molecules, all the different combinations of RDFs give relative positions of molecules as well as the intermolecular bonding information. We also calculated the first oxygen-hydrogen coordination numbers,

$$n_{\text{oh}} = 4\pi\rho \int_0^{\text{min}} g_{\text{oh}}(r) r^2 dr, \quad (8)$$

where  $g_{\text{oh}}$  is the oxygen-hydrogen RDF, and  $\rho$  is the number density. Hereafter, unless specified otherwise,  $\rho$  denotes the density in units of  $\text{g/cm}^3$ .

### 2. Dielectric constant and dipole moment

The dielectric constant  $\epsilon_r$  is directly related to the intermolecular orientational correlation and magnitude of each molecular dipole moment. The dielectric constant was calculated from the total dipole moment fluctuation [25,27]:

$$\epsilon_r = 1 + \frac{4\pi\rho\mu^2}{3k_B T} g_k. \quad (9)$$

In Eq. (9),  $k_B$  is the Boltzmann constant, and  $g_k$  is the Kirkwood factor, which can be obtained from the fluctuation of the total dipole moment [ $M = \sum (\mu + \mu^{\text{ind}})$ ] of the ensemble:

$$g_k = \frac{\langle M^2 \rangle}{N\mu^2}. \quad (10)$$

The Kirkwood factor is defined such that it has a value of unity if no orientational correlation is found. The evaluation of  $\epsilon_r$  depends on the treatment of the long-range electrostatic interactions. The Ewald sum [29] was used for long-range electrostatic interactions in the dielectric constant calculation, which is equivalent to tin-foil boundary conditions in the reaction field method; see Ref. [1] and references therein. As discussed elsewhere [28], this approximation introduces an additional uncertainty in the results. However, in practice the reported errors [1] are negligible. The total molecular dipole moment  $\mu_m$ , which has contributions from both the partial charge (permanent electric dipole equals 2.1936 D) and the induction interactions, is averaged over the entire ensemble:

$$\mu_m = \frac{1}{N} \sum_{i=1}^N (\mu_i + \mu_i^{\text{ind}}). \quad (11)$$

### C. Simulation details

Canonical NVT molecular dynamics simulations using the Shake algorithm [29] were performed for  $N = 500$  water molecules along the 1.0, 0.8, and  $0.6 \text{ g/cm}^3$  isochores in the 278–750 K temperature range. A cubic periodic simulation cell was used with fixed box lengths of 2.466, 2.654, and 2.921  $\text{\AA}$  for the 1, 0.8, and  $0.6 \text{ g/cm}^3$  isochores, respectively. The simulations were commenced from an initial face centered cubic lattice with a time step of 2 fs. The systems were equilibrated for 500 ps before any ensemble averages were determined. At each temperature, the total simulation time was at least 2 ns, which corresponds to  $1 \times 10^6$  time steps. The equations of motion were integrated using a leap-frog algorithm [29]. The Ewald summation method [29] was used to evaluate the long-range part of the Coulomb potential. The convergence parameter for the Ewald sum was  $\alpha = 5.0/L$ , with summation over  $5 \times 5 \times 5$  reciprocal lattice vectors, where  $L$  is the box length. The three-body interactions were truncated at  $L/4$  [20], and a cutoff of  $L/2$  is applied to the additive two-body interaction.

During the pre-equilibration stage, the temperature was held constant by rescaling the velocities every ten steps, which we found to be equivalent to results obtained using a Gaussian thermostat. To determine the induced dipole moment, a direct solver, namely, the conjugate gradient

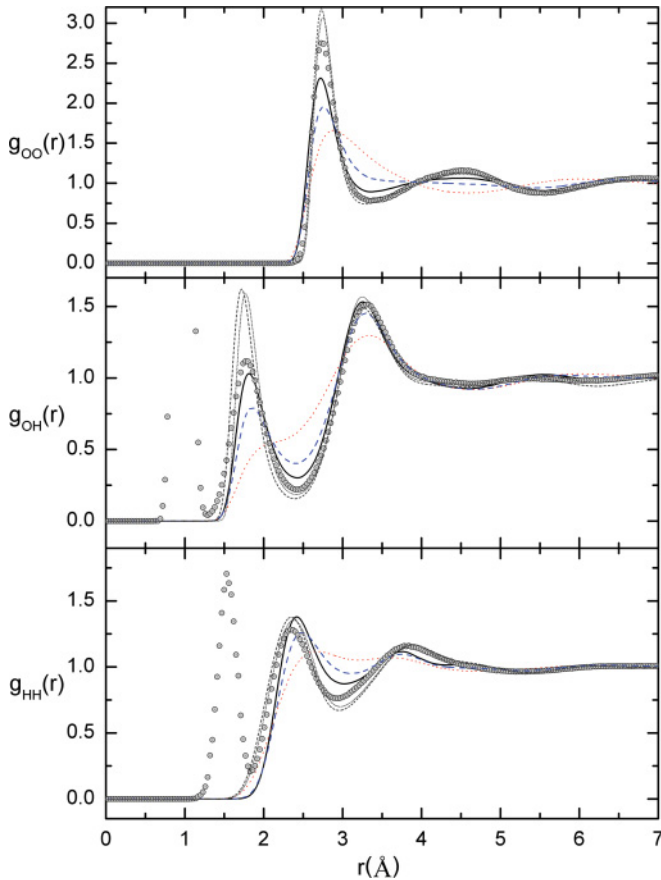


FIG. 2. (Color online) Temperature dependence of the oxygen-oxygen, oxygen-hydrogen, and hydrogen-hydrogen radial distribution functions along the  $1 \text{ g/cm}^3$  isochore obtained from the MCYna model (298 K, thick black line; 400 K, dashed blue line; 750 K, dotted red line). At  $T = 298 \text{ K}$ ,  $\rho = 1.0 \text{ g/cm}^3$  experimental data are available (gray circles) and a comparison at this temperature is also given for the SPC/E (gray short dotted line), and SPC/Fw (gray short dashed line) models.

method [30], was used. Ensemble averages were obtained by analyzing post-equilibrium configurations at intervals of 100 time steps and standard deviations were determined. The introduction of the induced dipole calculation and the Axilrod-Teller term significantly increases the computation load, requiring the implementation of a modified force decomposition algorithm [31] to parallelize the calculation. It was implemented with the MPI library, with more than 98% of the computational load distributed among 32 processors.

### III. RESULTS AND DISCUSSION

#### A. Structural properties along the isochores at 1, 0.8, 0.6 $\text{g/cm}^3$

##### 1. Radial distribution functions

Analyses have been carried out for bulk water along the 1, 0.8, and 0.6  $\text{g/cm}^3$  isochores in the temperature range of 278 to 750 K. Figure 2 shows the temperature dependence of oxygen-oxygen ( $g_{oo}$ ), oxygen-hydrogen ( $g_{oh}$ ), and hydrogen-hydrogen ( $g_{hh}$ ) RDFs for the  $\rho = 1 \text{ g/cm}^3$  isochore. For  $g_{oo}$  at 298 K, the positions of the first peak, second peak, and first

minimum are at 2.74, 4.53, and 3.36 Å, respectively, which are in good agreement with x-ray scattering [11,32], neutron diffraction measurements [14], and *ab initio* simulation of the IR spectrum of bulk water [33]. Such positions of the 2nd and the 1st peaks are ascribed to the local tetrahedral ice-like structure of the water. Thus, the peaks implicitly indicate the three-body correlation of oxygen atoms [1]. As temperature increases the 1st peak of  $g_{oo}$  broadens considerably, but its position remains essentially fixed with only a small outward shift. The second peak and the first minimum shift considerably from 4.53 and 3.36 Å at 298 K to 6.01 and 4.59 Å at 750 K, respectively. At 298 K, the 1st  $g_{oo}$  coordination shell is very thin, spanning from 2.74 to 3.36 Å, which suggests a layer of water molecules rather than a shell. In contrast at  $T = 750 \text{ K}$ , the 1st  $g_{oo}$  coordination shell is much thicker spanning from 2.74 to 4.59 Å, which is the middle of the 2nd shell at ambient temperature. Such behavior suggests that the local structure changes significantly with temperature. When the temperature rises above the normal boiling temperature, the second peak gradually flattens out and almost disappears in the supercritical region. Such temperature dependence of the 2nd peak indicates a gradual merging of the first and second coordination shells of water molecules with increasing temperature and pressure. This, in turn, indicates a significant reorganization of the H-bond network. Namely, the partial breaking of the total number of H-bonds and consequent transition of the structure of water from a tetrahedral to a more closely packed geometry. The ratio of the second peak position to the first one gives a measure of the local structure in the fluid. At 298 K, the ratio is 1.65, which is ascribed to the local tetrahedral coordination of the water molecules mentioned above. In contrast, at 750 K, the ratio is 2.1, which is equivalent to that of simple liquids such as argon [34].

The temperature dependence of the oxygen-hydrogen and hydrogen-hydrogen radial distribution functions illustrated in Fig. 2 is similar to that of oxygen-oxygen. When temperature and pressure are increased, the peaks broaden significantly and gradually shift toward larger intermolecular distances. The behavior of the  $g_{oh}$  first peak is the most interesting. Increasing the temperature results in the peak flattening out and eventually disappearing at  $T \geq 650 \text{ K}$ . The very sharp separation between the two OH shells and their position relative to the 1st OO peak at ambient conditions indicates a regular order in O-H orientations. For example, the 1st OH peak is located at 0.922 Å (the length of the O-H covalent bond in this model is 0.975 Å) behind the 1st OO peak, which means that the H atoms are orientated almost radially toward the O atom of the central water molecule. Increasing thermal energy diminishes the separation between the OH shells and at  $T \geq 650 \text{ K}$  they appear to merge into one shell. This means that most H atoms no longer have a preferred orientation relative to the neighboring molecules and are free to rotate around their own oxygen atom. The observed temperature dependence of  $g_{oh}$  indicates the collapse of the H-bond network at  $T \geq 650 \text{ K}$  for the MCYna model.

Figures 3 and 4 illustrate the temperature dependence of RDFs along the  $\rho = 0.8 \text{ g/cm}^3$  and  $\rho = 0.6 \text{ g/cm}^3$  isochores. The RDFs behave very much like in the case of  $\rho = 1 \text{ g/cm}^3$  with the first peaks broadening and the gradual disappearing of the 1st oxygen-hydrogen minima. The average intermolecular

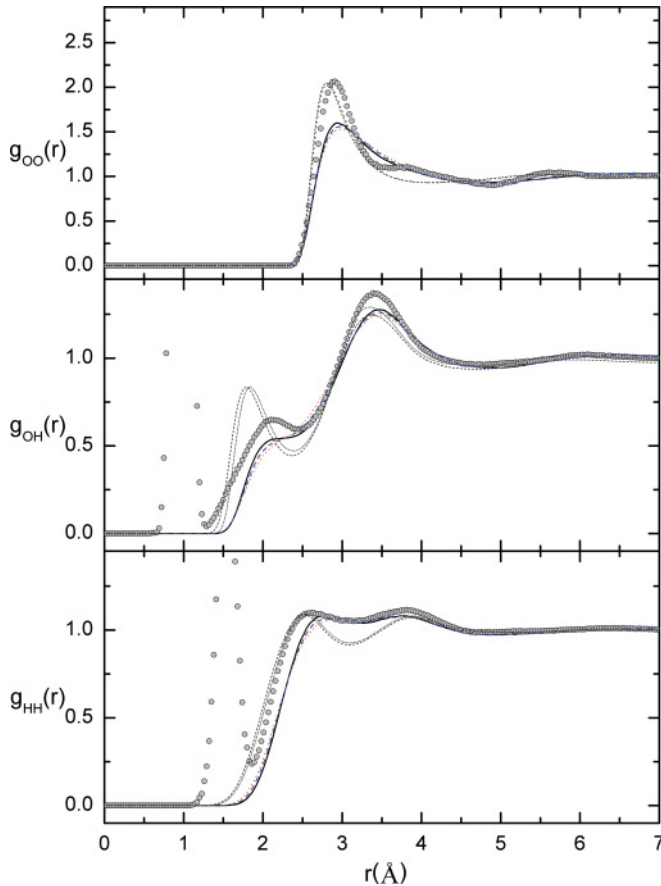


FIG. 3. (Color online) Temperature dependence of oxygen-oxygen, oxygen-hydrogen, and hydrogen-hydrogen radial distribution functions along the  $0.8 \text{ g/cm}^3$  isochore (573 K, thick black line; 650 K, blue dashed line; 750 K, red dotted line). At 573 K and  $\rho = 0.78 \text{ g/cm}^3$ , experimental data [14] are available (gray circles) and a comparison at this temperature is also given for the SPC/E (gray short dotted line), and SPC/Fw (gray short dashed line) models. Sharp peaks on the experimental  $g_{oh}$  and  $g_{hh}$  curves represent oxygen and hydrogen atoms of the same molecule.

distance for these isochores is larger than at  $\rho = 1 \text{ g/cm}^3$ , which manifests in peaks slightly shifted to the right. Another effect caused by the reduced density is the faster disappearance of the 1st  $g_{oh}$  minima with temperature. For example, at  $\rho = 0.8 \text{ g/cm}^3$  and  $\rho = 0.6 \text{ g/cm}^3$ , these minima vanish at approximately 550 and 450 K, respectively, whereas at  $1 \text{ g/cm}^3$  they disappear at 650 K.

In Figs. 2–4, simulations are compared with available NDIS experimental data [14] as well as with data from the SPC/E [6] and SPC/Fw [36] models. In general, RDFs for the  $1 \text{ g/cm}^3$  isochore coincide with experimental curves except the case of a smaller first  $g_{oo}$  peak. This feature was noticed by Niesar *et al.* [35] and can be explained by the fact that the MCY potential is too repulsive. This is due to the fact that very few configuration state functions were used for the computation of water dimer energies to obtain a good fit. However, the  $g_{oh}$  and  $g_{hh}$  values obtained from the MCYna model show much better agreement with experimental curves than the corresponding RDFs from nonpolarizable SPC/E [6] and SPC/Fw [36] models. RDFs for the  $0.8$  and  $0.6 \text{ g/cm}^3$  isochores show qualitative agreement

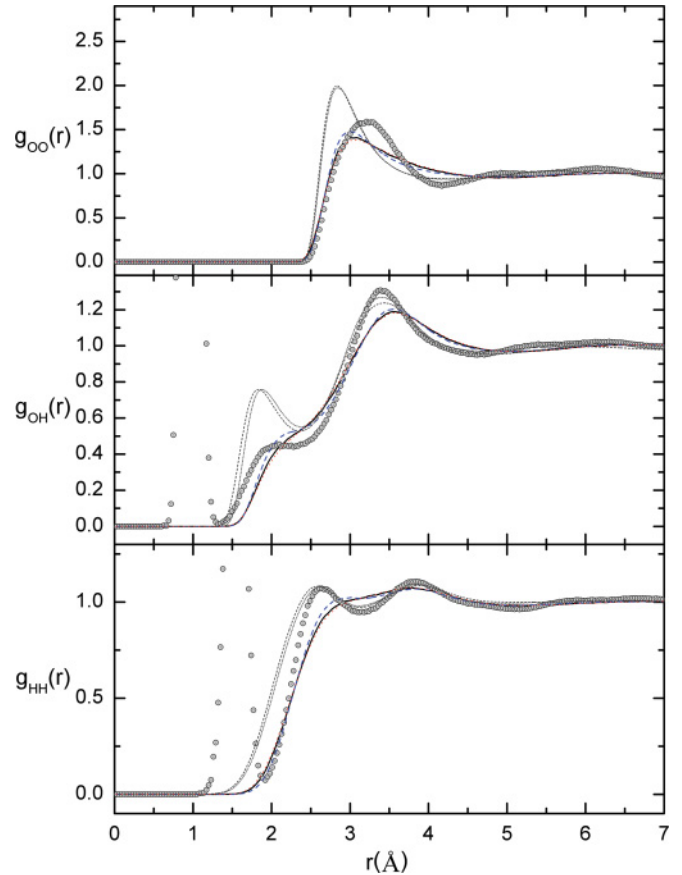


FIG. 4. (Color online) Temperature dependence of oxygen-oxygen, oxygen-hydrogen, and hydrogen-hydrogen radial distribution functions along the  $0.6 \text{ g/cm}^3$  isochore (550 K, blue dashed line; 673 K, thick black line; 750 K, red dotted line). At 673 K and  $\rho = 0.58 \text{ g/cm}^3$ , experimental data [14] are available (gray circles) and a comparison at this temperature is also given for the SPC/E (gray short dotted line), and SPC/Fw (gray short dashed line) models. Sharp peaks on the experimental  $g_{oh}$  and  $g_{hh}$  curves represent oxygen and hydrogen atoms of the same molecule.

with NDIS curves. Overall, comparing MD RDFs with the experimental data, we observed much greater preservation of the 1st and 2nd water shells at smaller densities than is predicted by MD simulations. These discrepancies can be attributed to the parameterization of the *ab initio* MCY model [20]. Originally, this model was developed with the help of configuration-interaction method to describe water properties at normal conditions.

## 2. Shell structure

Oxygen-hydrogen ( $n_{oh}$ ) coordination numbers together with RDFs allow better understanding of shell structure and H-bonding of water molecules at different densities and temperatures. Since the molecular structure in liquid water differs greatly from a regular crystal configuration, it is difficult to unambiguously define a fixed upper limit  $r_{min}$  for the integral in Eq. (8). In fact, the  $n_{oh}$  coordination number depends largely on the choice of this value. In this work, we accept the position of the first  $g_{oh}(r)$  minima as  $r_{min}$ . Thus,  $r_{min}$  means the size of the 1st oxygen-hydrogen solvation shell. Oxygen-hydrogen

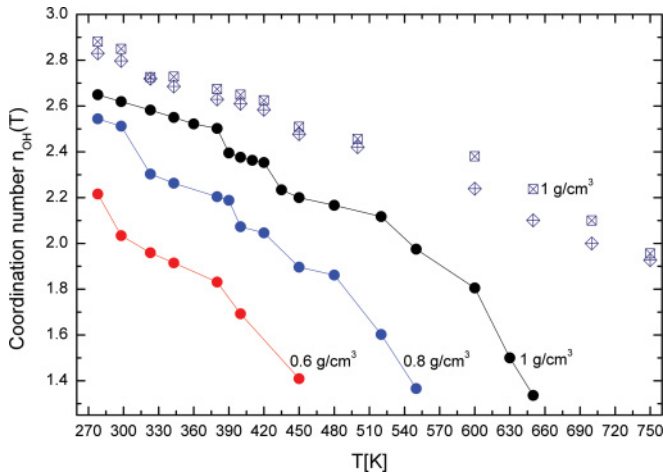


FIG. 5. (Color online) Evolution of the first oxygen-hydrogen coordination numbers with temperature. Results are plotted for the water along the 1, 0.8, and 0.6 g/cm<sup>3</sup> isochores (all circles). For comparison there are presented data from SPC/E model [6] (crossed squares) and SPC/Fw model [36] (crossed diamonds) along the 1 g/cm<sup>3</sup> isochore. The lines through the data points are given only for guidance.

( $n_{oh}$ ) coordination numbers for water along the 1, 0.8, and 0.6 g/cm<sup>3</sup> isochores are presented in Fig. 5. Starting from values of 2.71, 2.544, and 2.215 at 278 K, they gradually decrease to 1.336 at 650 K, 1.366 at 550 K, and 1.409 at 450 K, respectively. Interruption of  $n_{oh}$  is taking place due to the vanishing of the 1st  $g_{oh}$  minima at approximately 650, 550, and 450 K along each respective isochore.

This behavior of the 1st  $g_{oh}$  minima indicates the merging of water shells as a consequence of complete collapse of the H-bonding network. This indication of complete collapse of the H-bonding network seems to be premature and a characteristic only of the MCYna potential. We cannot infer the complete collapse of H-bond network from RDFs alone. More sophisticated calculations are required in order to estimate the number of remaining H-bonds. Molecular dynamics simulation results at  $\rho = 1$  g/cm<sup>3</sup> for other polarizable models show much better conservation of H-bond structure. For example, according to *ab initio* simulation of Kang *et al.* [9], tetrahedral H-bond network exhibits collapse above 800 K, whereas calculation with the TIP4P model [13] indicates that 70% of hydrogen bonds still remain at temperatures up to 1130 K. The number of hydrogen bonds obtained from nonpolarizable models like SPC/E (see Fig. 5) keep gradually decreasing well beyond 650 K. According to the MCYna potential, at  $T \geq 650$  K ( $\rho = 1$  g/cm<sup>3</sup>), almost half of the H-bonded molecules transform into interstitial molecules. The reason for the discrepancy between the potential models is due to the definition of the hydrogen bond. It is important to note that the  $n_{oh}$  coordination number is not exactly the number of hydrogen bonds. Equation (8) defines average number of molecules, which lie within a distance  $r_{min}$  from the central water molecule. As was shown by Kalinichev and Bass [37], this number coincides with number of H-bonds only at  $T \leq 500$  K. At higher temperatures and pressures geometrical criteria alone used in Eq. (8) are not sufficient. More elaborate criteria are required for the definition of

H-bonds over wider range of state points [8,37]. Taking such factors into consideration and despite the fact the quantitative assessment of the degree of hydrogen bonding is still a matter of debate, we can say that in real water at least some part of the H-bond network still exists even at supercritical temperatures.

The evaluation of oxygen-hydrogen coordination numbers along the 1 g/cm<sup>3</sup> isochore has also been performed for the rigid SPC/E [6] and flexible SPC/Fw [36] models. The comparison with the flexible water model is particularly important at high temperatures when the energy of intermolecular vibrations is comparable with  $k_B T$ . Incorporation of flexibility is intended to produce more realistic dynamic behavior of hydrogen bonds. It is apparent from Fig. 5 that these models give higher values of  $n_{oh}$ , which keep gradually decreasing well beyond 650 K. Introduction of bond flexibility does not significantly change  $n_{oh}$  compared to the rigid SPC/E model. However, as discussed above, SPC-based models overestimate the water structure, resulting in a 1st OH peak that is too high and an unrealistically sharp separation between the water shells, especially at lower densities. Taking into account the comparison between MD and experimental RDFs from Figs 2–4, it is apparent that the MCYna model yields more accurate  $n_{oh}$  values than the SPC-based models. It is also important to note that at lower densities it is difficult to calculate reliable  $n_{oo}$  and  $n_{oh}$  for nonpolarizable water models due to strong local density fluctuations.

We also calculated oxygen-oxygen coordination numbers ( $n_{oo}$ ) along the 1, 0.8, and 0.6 g/cm<sup>3</sup> isochores (see Table II). In the 278–373 K temperature region, the  $n_{oo}$  have very similar values, only increasing slowly with an increase on temperature. Along the 1 g/cm<sup>3</sup> isochore,  $n_{oo}$  starts from the classical value of 4.6 at 278 K and increases to approximately 4.9 at  $T = 373$  K. For the 0.8 g/cm<sup>3</sup> isochore,  $n_{oo}$  increases from 4.076 to 5.5. For the 0.6 g/cm<sup>3</sup> isochore,  $n_{oo}$  has values from 3.7 at 278 K to 4.5 at 373 K. The closeness of these coordination numbers in this temperature region indicates the presence of tetrahedral structure in water along the 0.8 and possibly 0.6 g/cm<sup>3</sup> isochores. However, in the temperature region shortly after normal boiling temperature and until approximately 400 K, a very sharp rise in the  $n_{oo}$  values occurs. After 400 K,  $n_{oo}$  slowly decreases to values of 12–13 at supercritical temperatures [34]. The reason for this discontinuity in  $n_{oo}$  values can be seen in the temperature dependence of oxygen-oxygen RDFs. In this region of intermediate temperatures, the RDFs ( $g_{oo}$ ) show characteristics that are specific to only the MCYna model. As is clearly seen from the  $g_{oo}$  values in Fig. 2, the 2nd peak, which represents the second coordination shell, vanishes with increased temperature and pressure. This indicates that the first two coordination shells are merging into one shell with a much more closely packed molecular structure. Merging shells make impossible proper determination of the integration limit  $r_{min}$  [see Eq. (8)]. The positions of the first OO and OH minima along the 1, 0.8, and 0.6 g/cm<sup>3</sup> isochores are presented in Table II. Many authors [8,9,13] use the positions of the 1st OO and OH minima at 298 K as criteria of H-bond formation. However, as is apparent from the data in Table II, these positions are not fixed but are temperature and density dependent. This effect imposes additional uncertainty on the choice of H-bond criteria.

TABLE II. Positions of the first minima of the MCYna RDFs together with  $n_{oo}$  values along the 1, 0.8, and 0.6 g/cm<sup>3</sup> isochores.

T [K]	1 g/cm <sup>3</sup>			0.8 g/cm <sup>3</sup>			0.6 g/cm <sup>3</sup>		
	O-O $r_{\min}$ [Å]	$n_{oo}$	O-H $r_{\min}$ [Å]	O-O $r_{\min}$ [Å]	$n_{oo}$	O-H $r_{\min}$ [Å]	O-O $r_{\min}$ [Å]	$n_{oo}$	O-H $r_{\min}$ [Å]
298	3.375	4.605	2.419	3.566	4.337	2.571	3.742	3.869	2.574
343	3.437	4.912	2.419	3.667	4.824	2.538	3.816	4.111	2.574
373	3.468	5.090	2.419	3.699	5.04	2.504	3.888	4.374	2.574
450	–	–	2.358	–	–	2.438	4.217	5.952	2.464
500	4.763	14.56	2.358	4.727	12.79	2.339	4.473	7.043	–
550	4.670	13.561	2.327	4.727	11.698	2.272	4.692	8.230	–
650	4.608	13.021	2.173	4.794	11.939	–	4.984	9.513	–
750	4.608	13.009	–	4.827	12.173	–	4.947	9.532	–

### B. Dielectric constant

Molecular dynamics and experimental static dielectric constants [38] are presented in Fig. 6. As expected,  $\epsilon_r$  is lower for higher temperatures. The temperature driven decrease of  $\epsilon_r$  is due to the reduction of molecular ordering. One of the main reasons for the high dielectric constant of water is that the extensive H-bond network enables a fast (within 10 ps) reorientation of the molecular dipoles in response to a field. Increasing the temperature increases the randomizing thermal fluctuations that oppose dipole alignment by an electrostatic field. Values of the dielectric constant  $\epsilon_r$  gradually decrease along all isochores. The decrease of  $\epsilon_r$  at lower densities is caused by strong local density fluctuations and is a consequence of a broken H-bond network and reduced polarizability of water.

Comparison with the experimental values of dielectric constant from elsewhere [38] shows that the MCYna model underestimates  $\epsilon_r$  by approximately 5% at temperatures lower than 343 K and overestimates  $\epsilon_r$  for the temperatures greater

than 450 K. In the temperature range 343–450 K MCYna predictions and experimental data almost coincide. Experimental results for 0.8 and 0.6 g/cm<sup>3</sup> isochores are available only in temperature regions of 550–750 K and 630–750 K, respectively. For lower temperatures we used an interpolation equation based on the experimental data collected in the work of Uematsu and Franck [39]. In the case of smaller water densities, MD results deviate more from experimental data than it was in case of  $\rho = 1$  g/cm<sup>3</sup>. Comparison with dielectric constants obtained from the SPC/E model is presented in Table III. The MCYna model gives better agreement with experiment for temperatures up to 400 K than the SPC/E model, which can be at least partly attributed to polarization interaction. Above the critical temperature, both polarizable MCYna and nonpolarizable SPC/E models give similar values of the dielectric constant. This trend can be explained by the fact that water at supercritical conditions behaves like a simple fluid, due to the collapse of the shell structure and significant reduction of the H-bond network.

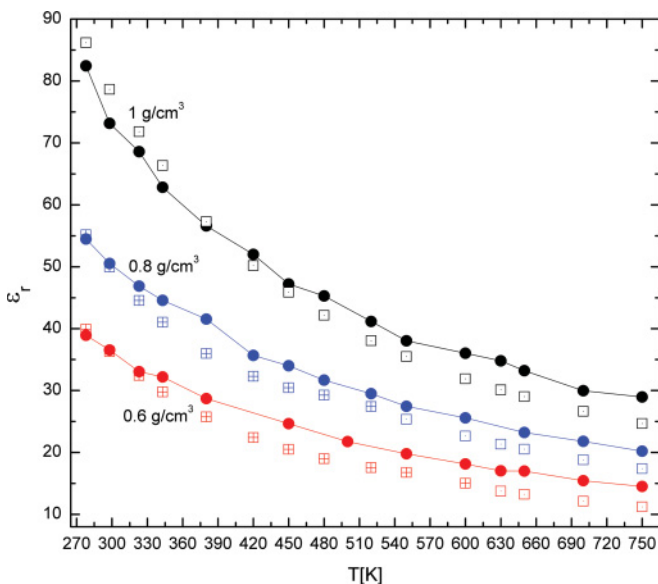


FIG. 6. (Color online) Temperature dependence of the static dielectric constant  $\epsilon_r$ . MD data along the 1, 0.8, and 0.6 g/cm<sup>3</sup> isochores (all circles). A comparison is given with both direct experimental data [38] (open squares) and interpolated experimental data [39] (crossed squares).

### C. Dipole moment

The effect of temperature on the polarization properties of liquid water is illustrated by the distribution of dipole moment of water molecules in Fig. 7. These distributions are obtained from an instantaneous snapshot at the end of the simulation run. The standard deviations for the 298, 480, and 700 K (1 g/cm<sup>3</sup> isochore) are 0.36, 0.29, and 0.28, respectively, and a comparison is given with the Gaussian distribution. The deviation from the Gaussian distribution reflects local fluctuation of molecular dipole at the given instance. The shape of the distributions, relative to the Gaussian distribution, was found to be widened toward the larger values of dipole moments. Peaks are also found to be shifted to the left from the mean values. These effects could be caused by the rigidity of the MCYna water molecule. The range of dipole values obtained from *ab initio* simulations [10,40] is usually quite close to a Gaussian distribution. As was shown in *ab initio* simulations [10,11], flexing of the molecule enhances the occurrence of the dipoles at the tails of the distribution. As temperature is increased, distributions become sharper and mean values shift toward smaller values of dipole moment. Comparing a given dipole distribution with the ones obtained from other *ab initio* [9,10] and MD simulations [8], we found the MCYna distributions to be much wider. They begin from

TABLE III. Static dielectric constants for the MCYna and SPCE models along the 1, 0.8, and 0.6 g/cm<sup>3</sup> isochores.

T [K]	1 g/cm <sup>3</sup>			0.8 g/cm <sup>3</sup>			0.6 g/cm <sup>3</sup>		
	Exp. $\epsilon_r$ [38]	MCYna	SPCE	Exp. $\epsilon_r$ [38]	MCYna	SPCE	Exp. $\epsilon_r$ [38]	MCYna	SPCE
278	86.175	82.435	70.161	–	54.484	–	–	38.919	–
298	78.65	73.161	66.380	–	50.537	–	–	36.528	–
323	71.80	68.583	61.109	–	46.87	–	–	33.052	–
343	66.34	62.833	57.824	–	44.567	–	–	32.189	–
380	57.29	56.609	52.213	–	41.53	–	–	28.703	–
400	53.53	53.205	49.647	–	37.89	40.116	–	27.287	–
450	45.875	47.21	44.237	–	33.99	35.786	–	24.644	–
500	40.00	43.102	40.027	–	30.49	32.299	–	21.758	–
600	31.89	36.021	33.528	22.65	25.586	27.052	–	18.132	20.532
650	29.015	33.196	31.013	20.54	23.22	25.072	13.235	16.99	19.071
750	24.66	28.947	27.021	17.38	20.207	21.873	11.21	14.507	16.641

a minimum value of 2.1936 D, which is assigned to the isolated water molecule according to MCY model [20] and span up to a value of 4.5 D. A similar trend was observed for dipole distributions of water along the 0.6 and 0.8 g/cm<sup>3</sup>

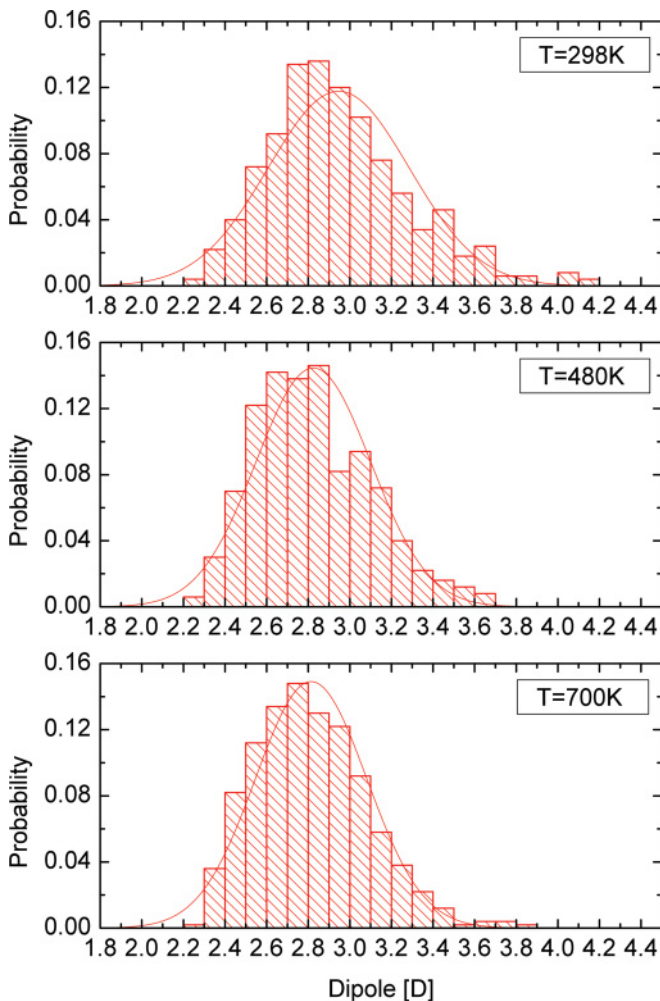


FIG. 7. (Color online) Distribution of dipole moments for water at 1g/cm<sup>3</sup> and temperatures 298, 480, and 700 K obtained from a single snapshot at the end of the simulation. Smooth curves show the corresponding Gaussian distributions.

isochores, which agree with previous *ab initio* [10] and MD [8] results.

Figure 8 shows the variation of average dipole moments at different densities as a function of temperature. Values of dipole moments gradually decrease with increasing temperature, slowly approaching stable values at supercritical temperatures. From Fig. 8 it is clearly seen that the average dipole moments are decreasing with decreasing density of water. This result is in qualitative agreement with recent *ab initio* simulations [10,12,27] and MD simulations [8]. The dipole moment calculated by Eq. (12) contains contributions from both the permanent dipole moment  $|\mu_i| = 2.1936$  D plus the induced dipole moment  $|\mu^{\text{ind}}|$ . In contrast to the gas phase, the internal electric field arising from the interaction of water molecules with its surroundings in the condensed phase polarizes molecules leading to large values of  $\mu^{\text{ind}}$  and a correspondingly large total dipole moment  $\mu$  [see Eq. (12)]. As discussed above, at densities  $\rho < 1$  g/cm<sup>3</sup>, average intermolecular distances are larger than at ambient conditions, and, therefore, polarization energy and average dipole moments should be smaller and slowly approach the

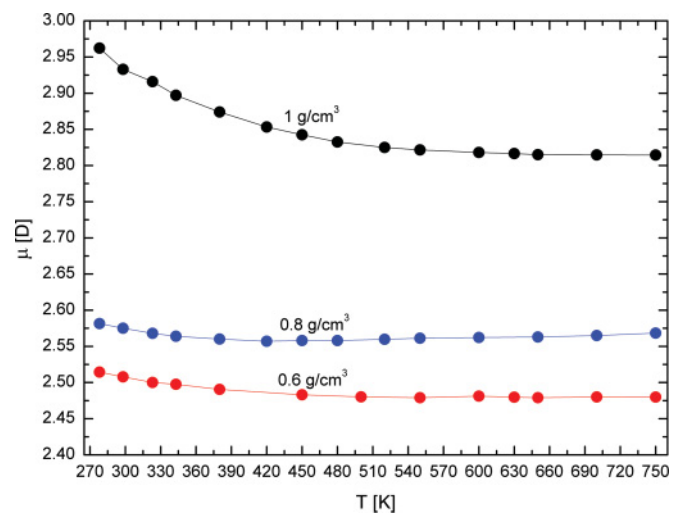


FIG. 8. (Color online) Temperature dependence of average dipole moments along the 1, 0.8, and 0.6 g/cm<sup>3</sup> isochores (all circles). The lines through the data points are given only for guidance.

vapor value of 1.89 D. The absence of reliable experimental data for the given temperatures and densities does not allow us to firmly establish correct temperature and density dependence of  $\mu$ .

#### IV. CONCLUSIONS

In this work we have examined the structure, dielectric, and polarization properties of the MCYna water model along the 1, 0.8, and 0.6 g/cm<sup>3</sup> isochores. In particular, we paid special attention to the effect of structural change of the fluid in the range from the normal boiling temperature up to the critical temperature. RDFs in general show good agreement with NDIS results [12,14]. Although SPC-based models yield better agreement with experiment for the height of the 1st OO peak, the MCYna model gives much better agreement of the 1st OH peak with the experimental curve, while SPC models significantly overestimate the peak height. In comparison to the MCYna model, nonpolarizable SPC-based models tend to overestimate structuring of water, particularly at high temperatures and low densities. Including polarizability improves the density-induced behavior of RDFs, although the 1st OH peaks still remain higher than observed experimentally. Along the 1 g/cm<sup>3</sup> isochore, the structure of water changes from a tetrahedral ice-like structure at room temperature to a simple liquid-like structure at higher temperatures. Although ice-like three-body correlation of water molecules largely vanishes at  $T \geq 373$  K, simple H-bonding between two molecules persists up until the critical temperature and beyond. At this temperature, the first peak of the oxygen-hydrogen

RDF vanishes, which makes impossible calculation of the oxygen-hydrogen coordination number. We conclude that up to 50% of the H-bonds are disrupted. Values of the first oxygen-oxygen coordination numbers along the 0.8 and 0.6 g/cm<sup>3</sup> isochores are reasonably close to values obtained at 1.0 g/cm<sup>3</sup> and temperatures less than or equal to 373 K. This indicates the presence of tetrahedral structure and H-bond network in bulk water at these densities and temperatures.

The static dielectric constant and average dipole moment change continuously along all isochores. Calculations confirmed the gradual decrease of the dielectric constant and average dipole moment with temperature and density. This trend is caused by a reduction of polarizability of the system, which in turn is caused by the collapse of the H-bond network and resulting thermal fluctuations that oppose dipole alignment by an electrostatic field. Dielectric constants calculated for water at normal density, and temperatures less than 450 K, agree within 5% of experimental values. Average dipole moments for water at ambient conditions seem to be in good agreement with *ab initio* calculations [10,12]. However, we also observed a very weak temperature dependence of the MCYna dipole moments at temperatures higher than 450 K. Calculated dipoles for  $\rho = 1$  g/cm<sup>3</sup> never fall below 2.81 D, while the dipole moments obtained from *ab initio* simulations dipoles fall to 2.6 D.

#### ACKNOWLEDGMENT

I.S. thanks Swinburne University of Technology for support through a postgraduate scholarship.

- 
- [1] J. Li, Z. Zhou, and R. J. Sadus, *J. Chem. Phys.* **127**, 154509 (2007).
- [2] D. Eisenberg and W. Kauzmann, *The Structure and Properties of Water* (Clarendon Press, Oxford, 1969).
- [3] F. Franks, in *Water: A Comprehensive Treatise*, edited by F. Franks (Plenum Press, New York, 1972), Vol. 1.
- [4] P. Ball, *Nature (London)* **452**, 291 (2008).
- [5] W. L. Jorgensen, J. Chandrasekhar, J. D. Madura, R. W. Impey, and M. L. Klein, *J. Chem. Phys.* **79**, 926 (1983).
- [6] H. J. C. Berendsen, J. R. Grigera, and T. P. Straatsma, *J. Phys. Chem.* **91**, 6269 (1987).
- [7] G. C. Lie and E. Clementi, *Phys. Rev. A* **33**, 2679 (1986).
- [8] N. Yoshii, H. Yoshie, S. Miura, and S. Okazaki, *J. Chem. Phys.* **109**, 4873 (1998).
- [9] D. Kang, J. Dai, and J. Yuan, *J. Chem. Phys.* **135**, 024505 (2011).
- [10] P. J. Dyer and P. T. Cummings, *J. Chem. Phys.* **125**, 144519 (2006).
- [11] M. Allesch, E. Schwegler, F. Gygi, and G. Galli, *J. Chem. Phys.* **120**, 5192 (2004).
- [12] T. Ikeda, Y. Katayama, H. Saitoh, and K. Aoki, *J. Chem. Phys.* **132**, 121102 (2010).
- [13] R. D. Mountain, *J. Chem. Phys.* **90**, 1866 (1989).
- [14] A. K. Soper, *Chem. Phys.* **258**, 121 (2000).
- [15] R. H. Tromp, P. Postorino, G. W. Neilson, M. A. Ricci, and A. K. Soper, *J. Chem. Phys.* **101**, 6210 (1994).
- [16] G. Loffler, H. Schreiber, and O. Steinhauser, *Ber. Bunsen-Ges. Phys. Chem.* **98**, 1575 (1994).
- [17] G. Weck, J. Eggert, P. Loubeyre, N. Desbiens, E. Bourasseau, J.-B. Maillet, M. Mezouar, and M. Hanfland, *Phys. Rev. B* **80**, 180202(R) (2009).
- [18] E. R. Batista, S. S. Xantheas, and H. Jonsson, *J. Chem. Phys.* **109**, 4546 (1998).
- [19] R. Car and M. Parrinello, *Phys. Rev. Lett.* **55**, 2471 (1985).
- [20] O. Matsuoka, E. Clementi, and M. Yoshimine, *J. Chem. Phys.* **64**, 1351 (1976).
- [21] G. Marcelli and R. J. Sadus, *J. Chem. Phys.* **111**, 1533 (1999).
- [22] B. M. Axilrod and E. Teller, *J. Chem. Phys.* **11**, 299 (1943).
- [23] P. J. Leonard and J. A. Barker, in *Theoretical Chemistry: Advances and Perspectives*, edited by H. Eyring and D. Henderson (Academic Press, London, 1975), Vol. 1.
- [24] C. A. Coulson and D. Eisenberg, *Proc. R. Soc. London, Ser. A* **291**, 445 (1966).
- [25] C. G. Gray and K. E. Gubbins, *Theory of Molecular Fluids* (Clarendon, Oxford, 1984), Vol. 1.
- [26] U. Niesar, G. Corongiu, E. Clementi, G. R. Kneller, and D. K. Bhattacharya, *J. Phys. Chem.* **94**, 7949 (1990).
- [27] M. Sharma, R. Resta, and R. Car, *Phys. Rev. Lett.* **98**, 247401 (2007).
- [28] M. Neumann, *Mol. Phys.* **50**, 841 (1983).

- [29] R. J. Sadus, *Molecular Simulation of Fluids: Theory, Algorithms and Object-Oriented* (Elsevier, Amsterdam, 1999).
- [30] G. Karniadakis and R. M. Kirby, *Parallel Scientific Computing in C and MPI: A Seamless Approach to Parallel Algorithms and their Implementation* (Cambridge University Press, Cambridge, 2003).
- [31] J. Li, Z. Zhou, and R. J. Sadus, *Comput. Phys. Commun.* **175**, 683 (2006).
- [32] J. M. Sorenson, G. Hura, R. M. Glaeser, and T. Head-Gordon, *J. Chem. Phys.* **113**, 9149 (2000).
- [33] M. Heyden, J. Sun, S. Funkner, G. Mathias, H. Forbert, M. Havenith, and D. Marx, *Proc. Natl. Acad. Sci. USA* **107**, 12068 (2010).
- [34] M. S. John and H. Eyring, *Ann. Rev. Phys. Chem.* **27**, 45 (1975).
- [35] U. Niesar, G. Corogniu, E. Clementi, G. R. Kneller, and D. K. Bhattacharya, *J. Phys. Chem.* **94**, 7949 (1990).
- [36] Y. Wu, H. Tepper, and G. Voth, *J. Chem. Phys.* **124**, 024503 (2006).
- [37] A. G. Kalinichev and J. D. Bass, *Chem. Phys. Lett.* **231**, 301 (1994).
- [38] D. P. Fernandez, A. R. H. Goodwin, E. W. Lemmon, J. M. H. Levelt Sengers, and R. C. Williams, *J. Phys. Chem. Ref. Data* **26**, 1125 (1997).
- [39] M. Uematsu and E. Franck, *J. Phys. Chem. Ref. Data.* **9**, 1291 (1980).
- [40] J. Sun, D. Bousquet, H. Forbert, and D. Marx, *J. Phys. Chem.* **133**, 114508 (2010).